Ann. Geophys., 29, 2305–2316, 2011
www.ann-geophys.net/29/2305/2011/
doi:10.5194/angeo-29-2305-2011

Annales Geophysicae

A mechanism for heating electrons in the magnetopause current layer and adjacent regions

A. Roux[1], P. Robert[1], O. Le Contel[1], V. Angelopoulos[2], U. Auster[3], J. Bonnell[4], C. M. Cully[5], R. E. Ergun[6], and J. P. McFadden[4]

[1]LPP-CNRS, UMR7648, Ecole Polytechnique, route de Saclay, 91128 Palaiseau cedex, France
[2]IGPP/ESS University of California, Los Angeles, CA, 90095-1567, USA
[3]Institut fur Geophysik und extraterrestrische Physik der Technischen University at Braunschweig, Mendelssohnstrasse 3, 38106 Braunschweig, Germany
[4]Space Sciences Laboratory, University of California, Berkeley, 7 Gauss Way, Berkeley, CA, 94720-7450, USA
[5]Department of Physics, Umeå University, Umeå, Sweden
[6]Department of Astrophysical and Planetary Sciences, University of Colorado, Boulder, CO 80309, USA

Received: 30 June 2011 – Revised: 30 September 2011 – Accepted: 10 November 2011 – Published: 23 December 2011

Abstract. Taking advantage of the string-of-pearls configuration of the five THEMIS spacecraft during the early phase of their mission, we analyze observations taken simultaneously in the magnetosheath, the magnetopause current layer and the magnetosphere. We find that electron heating coincides with ultra low frequency waves. It seems unlikely that electrons are heated by these waves because the electron thermal velocity is much larger than the Alfvén velocity (V_a). In the short transverse scale ($k_\perp \rho_i >> 1$) regime, however, short scale Alfvén waves (SSAWs) have parallel phase velocities much larger than V_a and are shown to interact, via Landau damping, with electrons thereby heating them. The origin of these waves is also addressed. THEMIS data give evidence for sharp spatial gradients in the magnetopause current layer where the highest amplitude waves have a large component δB perpendicular to the magnetopause and k azimuthal. We suggest that SSAWs are drift waves generated by temperature gradients in a high beta, large T_i/T_e magnetopause current layer. Therefore these waves are called SSDAWs, where D stands for drift. SSDAWs have large $k_\perp$ and therefore a large Doppler shift that can exceed their frequencies in the plasma frame. Because they have a small but finite parallel electric field and a magnetic component perpendicular to the magnetopause, they could play a key role at reconnecting magnetic field lines. The growth rate depends strongly on the scale of the gradients; it becomes very large when the scale of the electron temperature gradient gets below 400 km. Therefore SSDAW's are expected to limit the sharpness of the gradients, which might explain why Berchem and Russell (1982) found that the average magnetopause current sheet thickness to be ∼400–1000 km (∼500 km in the near equatorial region).

Keywords. Magnetospheric physics (Magnetopause, cusp, and boundary layers; Magnetosheath) – Space plasma physics (Wave-particle interactions)

1 Introduction

Intense ULF electromagnetic waves (0.2-5Hz) have been regularly observed by spacecraft crossing the magnetopause and adjacent layers (Anderson et al., 1982; Rezeau et al., 1986). To determine the nature of these fluctuations, Rezeau et al. (1993) made correlations between the two ISEE spacecraft and showed that the short-lived, intense, electromagnetic fluctuations observed near the magnetopause (∼few nT, corresponding to $\delta B/B$ up to 1–15 %) correspond to non-linear kinetic Alfvén wave (KAWs) structures moving along the magnetopause. A similar conclusion was drawn by Stasiewicz et al. (2000), who investigated the electric and the magnetic signatures of these waves and suggested that they correspond to kinetic Alfvén waves affected by a large Doppler shift. Using Themis data taken near the magnetopause Chaston et al. (2008) have estimated the perpendicular wave lengths; they showed that the wavelengths are very small ($k_\perp \rho_i > 1$) and that these Alfvénic fluctuations can transport magnetosheath plasma through the magnetopause at about the Bohm rate. There is as yet no consensus about the process that generates KAWs in the magnetopause layers. Stasiewicz et al. (2000) suggested that these fluctuations

Correspondence to: P. Robert
(patrick.robert@lpp.polytechnique.fr)

are coupled via drift effects to strong density gradients developing at the magnetopause. Belmont and Rezeau (2001) proposed a mechanism where KAWs are produced by mode conversion, in the density gradients of the magnetopause and adjacent layers, of fast modes carried by the solar wind. Chaston et al. (2008) suggest that KAWs are one of the by-product of magnetic reconnection.

The AMPTE-UK spacecraft has regularly observed heated electron at the magnetopause (Mp) and adjacent layers. According to Hall et al. (1991) this heating could be due to wave activity in the ULF range. In some of the events, heated electrons were found to be counter-streaming in parallel and anti-parallel directions. Thus both electron heating and enhanced wave activity are known to occur at the Mp and adjacent layers but the potential relation between them remains to be investigated. As indicated above, data analysis suggests that the observed fluctuations correspond to Alfvén waves. Yet Alfvén waves are expected to move at parallel phase velocities on the order of the Alfvén velocity ($V_a \sim 100\,\mathrm{km\,s^{-1}}$), which is much lower than the electron thermal velocity. Thus, a resonant interaction between electrons and Alfvén waves is not expected to occur. Therefore electrons are not (a priori) expected to be heated by the waves. Recently, however, Howes et al. (2008) have ran kinetic simulations showing that the phase velocity of KAWs gets much larger than V_a, when $k_\perp \rho_i \gg 1$. In this regime KAWs can efficiently interact with electrons for instance via Landau damping. Using interferometric methods Sahraoui et al. (2008) have analyzed the k-spectra of magnetic fluctuations measured in the solar wind by the four Cluster spacecraft. They also interpreted the observed fluctuations as small scale ($k_\perp \rho_i \gg 1$) KAWs, and showed that they can have scales so small that they can interact via Landau or cyclotron damping with solar wind electrons. In their interpretation small-scale KAWs are produced by a cascade (down to the electron scale) of large scale Alfvén waves generated near the Sun. In the magnetopause current layer (MpCL), however, strong perpendicular gradients will tend to inhibit the evolution towards a fully developed cascade.

Here we investigate a direct generation mechanism via a linear instability driven by steep gradients. After a short description of the instruments and the context (Sect. 2), we give evidence for the link between intense waves observed near the MpCL and electron heating (Sect. 3). The characteristics of the observed electromagnetic fluctuations are described in Sect. 4. In Sect. 5 we seek to identify the free energy source that drives the observed waves unstable. Conclusions are presented in Sect. 6.

2 Instrumentation and context

Here we use data from four instruments on board the five THEMIS spacecraft Tha, Thb, Thc, Thd and The). Descriptions of these instruments and early results can be found in Angelopoulos et al. (2008), Auster et al. (2008), Bonnell et al. (2008), Mc Fadden et al. (2008), Roux et al. (2008), Le Contel et al. (2008). Unfortunately the commissioning of EFI, the Electric Field Instrument, was not finished when the event we selected occurred; only Thc E-field data could be obtained. Electric field measurements being available on Thc, the spacecraft potential could be calculated and used to remove photo electron contamination for this spacecraft. Thus the electron temperature T_e was measured during the whole period on Thc. On Thb and Thd, however, the lack of E-field measurement made it impossible to remove photo-electron effects while these s/c were in the low density, hot magnetospheric plasma. Yet when the density was large, as in the MpCL, or in the magnetosheath (MSh), T_e could be measured. Thc electric and magnetic filter bank data (Cully et al., 2008) are available in 6 logarithmically-spaced frequency bands from 0.1 Hz to 4 kHz, with one measurement every 4 s.

20 May 2007 was selected because on that date the five spacecraft were near the dayside magnetopause and were in a string-of-pearls configuration. It was therefore possible to measure simultaneously the properties of the plasma (i) outside the magnetopause, in the adjacent magnetosheath (MSh), (ii) inside the magnetopause current layer (MpCL), and (iii) inside the adjacent magnetosphere (MSp). While crossing the magnetopause and adjacent regions, the five spacecraft have recorded the signatures of a flux transfer event (FTE). This FTE and the overall characteristics are described by Sibeck et al. (2008). Here it is sufficient to keep in mind that the 5 spacecraft were essentially aligned along the XGSE direction and located in the afternoon sector, as shown on Fig. 1.

Because Tha and The were very close and give similar results, we only display data from Tha, and skip data from The. The same is true for Thc and Thb. Thus on Figs. 2 and 3 we have display data from Tha (located in the adjacent MSh), Thd (remaining for a long time in the MpCL), and Thb (MSp). As electric data are only available on Thc, we use Thc (Fig. 5) to estimate the $\delta E/\delta B$ ratio, and identify electron temperature gradients.

3 Heating of particles

3.1 Electron heating

Figure 2 shows the 3 components of the magnetic field measured by the fluxgate magnetometer, magnetic fluctuations from the search-coil, and an electron spectrogram (up to about 20 keV), from Thb, Thd and Tha. Below we describe data gathered by each of the spacecraft.

– During most of the time interval Thb (top 3 panels) was located in the MSp, as indicated by the positive B_z component, and by a modest flux of energetic (few keV) electrons. Inside the region bracketed by pink lines

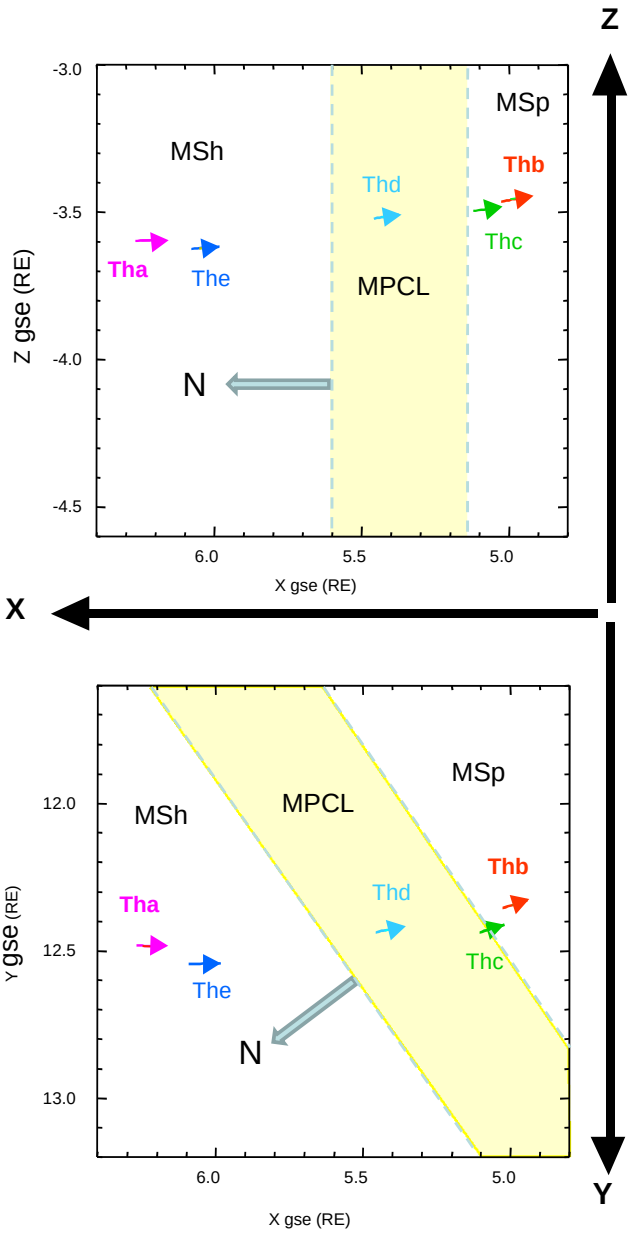

Fig. 1. Positions of the 5 THEMIS spacecraft in XZ (top) and XY (below) GSE coordinates, as indicated by colored arrows. Notice that the Y and Z coordinates are about the same for all the spacecraft. Their locations are spread along the X direction. Dotted lines suggest possible boundaries of the MpCL and illustrates the bracketing of the MpCL. The XZ plane is a cut for $y \approx 12.5\,R_E$ (corresponding to the locations of the spacecraft). Given the size of the region displayed, no attempt wase made to take field lines curvature into account.

(22:02:00–22:02:30), we observe electrons with lower energies than in the adjacent MSp, but much larger fluxes, and the magnetic signature of the FTE mentioned earlier.

– Before 21:59:15 Thd is also located in the MSp. It penetrates in the MpCL and returns to the MSp after 22:04:00. Yet Thd remained much longer (about 5 mn) in the MpCL than Thb, and gathered data, not only during the crossing of the FTE, but also in the MpCL. In the corresponding region (also bracketed by pink vertical lines), the average magnetic field, measured onboard Thd is weak and the fluctuations are intense, particularly after crossing the FTE. Note that energy distribution of the electron flux is the same as in the bracketed region of Thb. Inside the bracketed regions of Thb and Thd (the MPCL), $T_e \approx 60$ eV

– Before 22:01:45 and after 22:03:15 UT, Tha was located in the MSh, as indicated by a large flux of very low-energy electrons with a temperature of ∼35 eV (see Fig. 5) and confirmed by a negative B_z. As the FTE moved along the magnetopause (Mp), the MpCL thickened and Tha got closer to it (see the model by Sibeck et al., 2008). This close approach corresponds to the region bracketed in pink in which the electron spectrogram gives evidence for (i) a very low flux of energetic (magnetospheric) electrons and an increase in the temperature of low energy (magnetosheath) electrons. Their temperature (∼60 eV) is almost twice that of the adjacent free MSh; they are identified as heated MSh electrons. Hence electrons are efficiently heated as they approach/penetrate the MpCL. Electrons observed by Tha, Thb and Thd in the pink bracketed regions are very similar in terms of fluxes, temperatures and densities (see Fig. 3). These densities are the same as in the MSh but temperatures are enhanced, suggesting that electrons observed in the MpCL at Thb and Thd are heated MSh electrons, as confirmed by data shown in Fig. 3, for densities and Fig. 5 for temperatures.

Note that the 3 bracketed regions, in which high fluxes of heated electrons are observed coincide with enhanced wave intensities (typically in a frequency range 0.2–5 Hz), which leads to suspect that these intense waves ($\delta B \sim 1$ nT corresponding to $\delta B/B \sim 10\,\%$) heat electrons.

3.2 Weak ion heating

Figure 3 is in the same format as Fig. 2, but for ions. Ion densities and temperatures are plotted for Thb, Tha and Thd, together with the magnetic field and an ion spectrogram. The weak fluxes of energetic ions and the low densities (∼0.1–0.2 cm^{-3}) observed on both sides of the bracketed regions of Thb and Thd confirm that they were in the MSp before and after crossing the MpCL. As for electrons, enhanced fluxes of ions are found inside the pink bracketed periods, by Thb and Thd. On Tha, however, the ion spectrogram observed during the bracketed period is almost the same as in the adjacent MSh on both sides of the bracketed region. The last panel of Fig. 3 confirms that the ion temperature (T_i) only weakly

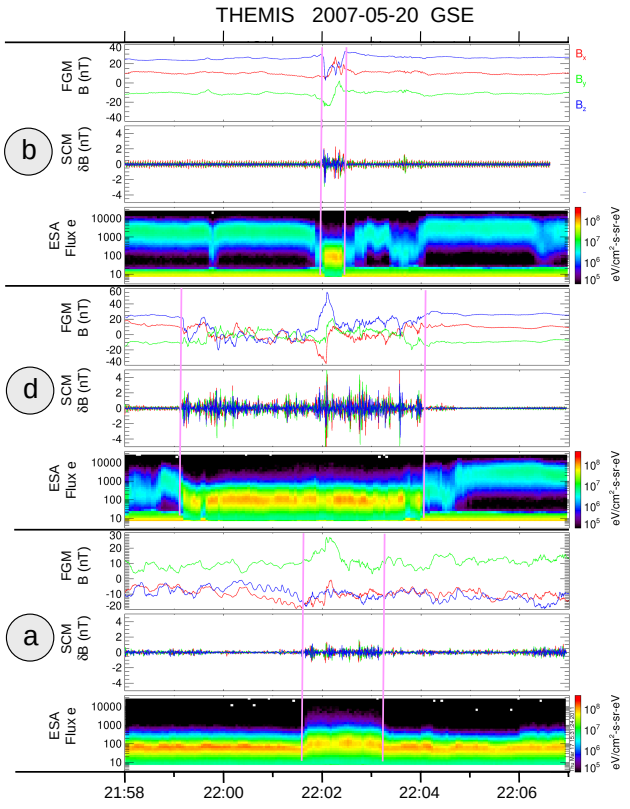

Fig. 2. Composite showing 3 sets of 3 panels. Each set corresponds to one spacecraft: Thb (top), Thd, (mid) and Tha (lower). Within each set we display data from the fluxgate (top), search coil (mid) and an electron spectrogram from ESA (bottom panel). Large electrons fluxes are observed on Thb and Thd between vertical lines. Large fluxes of heated electrons are also observed on Tha (lowest panel). Within the bracketed region, the electron temperatures ($T_e \sim 60$ eV) at Tha, is larger than in the adjacent free MSh ($T_e \sim 35$ eV). The electron temperature is the same ($T_e \approx 60$ eV) within the 3 bracketed regions, for Tha, Thb and Thd. Notice that the large fluxes of heated electrons coincide with enhanced wave amplitudes (see text).

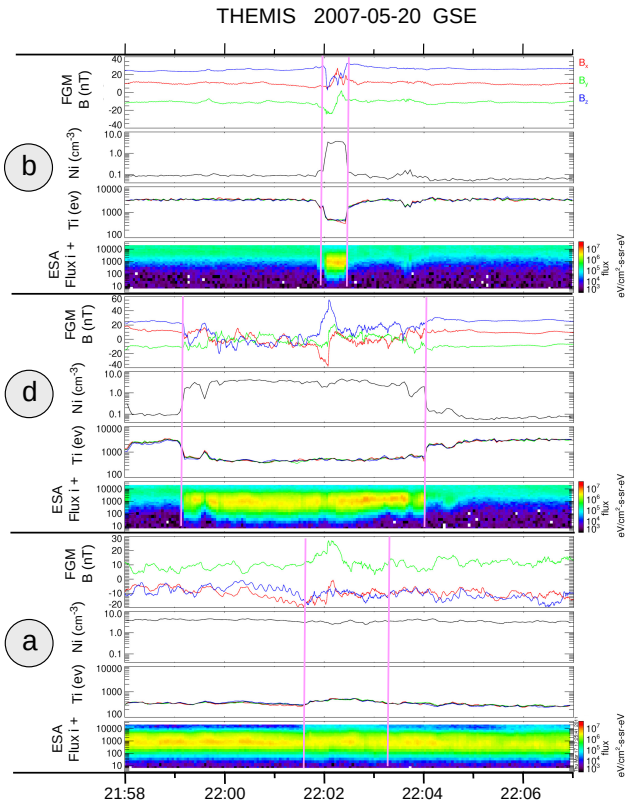

Fig. 3. Composite showing (i) the magnetic field, (ii) the ion density, (iii) the ion temperature, and (iv) an ion spectrogram, for Thb, Thd, and Tha respectively. As Tha approaches the MpCL the ion temperature variation remains small (see last panels). The ion temperatures at Thb and Thc in the MpCL (between vertical lines) are almost the same as the ion temperature measured by Tha in the free MSh. Note that the ion density inside the bracketed regions (which corresponds to MpCL) of Thb and Thd is about the same as in the MSh (Tha).

increases, from ∼400 eV to ∼500 eV. The ion density (N_i) measured by Tha does not change significantly as it crosses the bracketed region. Thus T_i and N_i are about the same within the 3 bracketed regions and almost the same as MSh values. The lack of variation in N_i and T_i tells us that MSh ions have penetrated the MPCL (and FTE) with little change in their density and temperature. On the other hand, MSh electrons also penetrate the MpCL (see discussion in Sect. 2), but their temperature increases by almost a factor of 2. We will now investigate the potential role of the waves observed in the MpCL by the 3 spacecraft, on electron heating. Let us first determine the nature of the fluctuations.

4 Characterization of the fluctuations

4.1 Polarization

It is convenient to use the same coordinate system for the 5 spacecraft whether they are far from or close to the magnetopause. The TPN coordinate system used here is defined geometrically; it has two axes tangent to a paraboloid (with the symmetry of revolution) passing by the spacecraft and by the subsolar point defined from the Tsyganenko 89 model, taken for the Kp of the day of the event. A representation of the TPN is given in Fig. 4. Unlike the MVA the TPN is not influenced by the crossing of the FTE. To make a meaningful comparison between MVA and TPN, we determined the MVA frame from the analysis of FGM data for the period preceding the FTE: 21:50 to 22:02 UT (with a 12 s average); for Thd which remains longer in the MpCL than its companions. The matrix from MVA to GSE and the matrix from MVA to TPN are given in Table 1. The normal

component of the TPN coordinate system almost coincides with the normal obtained via MVA. This normal is close to be in the XYgse plane. The T component (of the TPN) is close to the M component (of LMN), whereas P (of TPN) is close to L (of LMN). Figure 5 shows magnetic fields and flow velocities in the TPN coordinate system, along with ion densities. In the MSp, B_T is positive but B_P is negative, as expected. Conversely, B_T is negative and B_P positive in the MSh. Note also that B_N fluctuates around zero in the MpCL (Thd). On both sides of the event (in the MSp), the B_N component is almost null for Thb and Thd which illustrates the value of the TPN coordinates for describing magnetopause crossings. Because Thd spent a relatively long time in the MpCL and crossed the FTE, it is interesting to compare the ion velocity in both cases. We find maxima of the ion drift velocity $|V_d|$ well before and well after the FTE. During these two periods $|V_d|$ reaches 350 km s^{-1}, well above MSh values ($\sim$250 km s^{-1}).

Table 2 (top) shows the results of MVA carried out on the waves magnetic component measured by the fluxgate magnetometer aboard Thd, between 22:02:45 and 22:03:30. This period was chosen because the averaged dc magnetic field (Bdc) does not vary too much, it is therefore possible to relate the directions of variance to the direction of Bdc and thus determine the polarization. During this period the plasma velocity is accelerated; this acceleration corresponds to the largest wave intensities. The maximum variance of the waves is along N; the intermediate variance is along P; and the minimum variance is along T. For the sake of verification MVA has also been applied to search coil data filtered between 0.8 and 4 Hz, the maximum frequency covered by the instrument during this event. The normal (Nw) obtained by MVA applied to both instrument is almost the same, as can be seen from Table 2 (bottom). The waves propagate along the magnetopause in the azimuthal direction.

Thus the fluctuations measured by Thd have a large component normal to the Mp, and they propagate essentially in the azimuthal direction. Between 22:02:45 and 22:03:30, Bdc is essentially along P.

4.2 Nature of the waves

As shown in the previous subsection, the dominant component of the wave is along N (maximum variance), with a smaller (compressional) component along P, which is close to the direction of Bdc froml 22:02:45–22:03:30. The wave number k (minimum variance) is tangent to the magnetopause, essentially in the azimuthal direction, and therefore it is almost perpendicular to Bdc. Thus we conclude that $k_\perp \gg k_{//}$. In such a situation a compressional/magnetosonic wave would have: $\delta B // Bdc$ while we find that the dominant δB (maximum variance) is perpendicular to Bdc, which suggests that the observed waves are Alfvénic. How then can we explain the interaction with electrons? A resonant interaction between electrons and a classical Alfvén wave is not expected to occur because the electron thermal velocity ($V_e \sim 2000$ km s^{-1}, $T_e \sim 30$ eV) is much larger than the wave phase velocity ($\omega/k_{//} \sim V_a \sim 100$ km s^{-1}, for $Bo \sim 10$ nT and $N_o \sim 4$ cm^{-3}).

Electric field measurements can help resolve this paradox. As indicated earlier Thd E-field measurements were not yet available (commissioning). Electric field data were already available on Thc, however. Thc filterbank data are shown in Fig. 6. Panel (a) gives the dc magnetic field, and panel (b) shows the $\delta E/\delta B$ ratio for different frequencies ranging from 3 to 192 Hz, together with V_a. We find that $\delta E/\delta B \gg V_a$ at all frequencies over the entire period; for 3 Hz, $(\delta E/\delta B)/V_a$ is at least 5, and much larger for higher frequencies (in fact smaller scales as will be explained later). For an Alfvén wave $\delta E/\delta B \sim \omega/k_{//}$; therefore $\delta E/\delta B \gg V_a$ implies $\omega/k_{//} \gg V_a$.

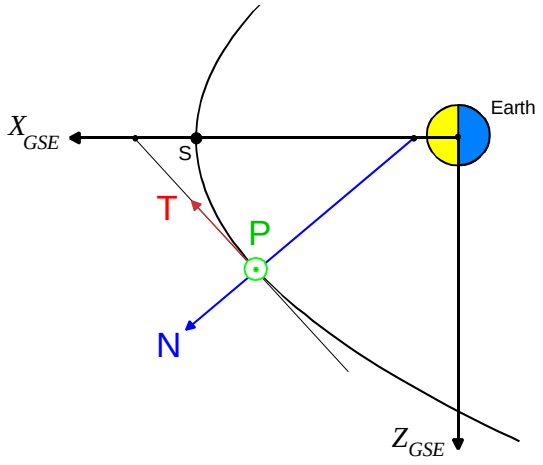

Fig. 4. Sketch showing the TPN (tangent, perpendicular, normal) coordinate system. T and P are tangent and N normal to a paraboloid passing by the spacecraft and by the subsolar point defined from the Tsyganenko 89 model taken for the Kp of the day of the event.

Table 1. Top: directions (in GSE) of the axis of variance obtained from MVA applied to flux gate data during Mp crossing. Bottom: direction (in MVA frame) of the TPN axis (see Fig. 4 and text).

λ_1	λ_2	λ_3	
0.985933	0.162937	0.037247	
M	V	A	
0.433616	−0.424103	0.795056	G
−0.566234	0.558119	0.606533	S
−0.700968	−0.713190	0.001868	E
T	P	N	
0.537986	0.828793	0.153870	L
−0.842603	0.534009	0.069719	M
−0.024387	−0.167162	0.985626	N

Table 2. Top: directions of the axis of variance obtained from MVA applied to Thd flux-gate data filtered between 0.8 and 2Hz (the maximum frequency covered during this event). Bottom: same for search-coil data filtered between 0.8 and 4 Hz. Results are given in TPN coordinates (see Fig. 4 and text). Lw, Mw and Nw are the LMN components of the waves.

λ_1	λ_2	λ_3	FGM
1.000000	0.693723	0.523545	
T	P	N	
−0.138757	0.066091	0.988119	Lw
−0.383818	−0.923375	0.007862	Mw
0.912924	−0.378167	0.153492	Nw
λ_1	λ_2	λ_3	SCM
1.000000	0.826541	0.456823	
T	P	N	
−0.078937	0.620455	0.780260	Lw
−0.301319	0.731241	−0.611959	Mw
−0.950250	−0.283413	0.129233	Nw

In addition to data from Thc, Fig. 6 panel (d) shows T_e from Tha. Electric field measurements were not yet available on Tha. Yet because Tha was mostly in the MSh and MpCL (dense plasmas), T_e could be measured safely. We observe that $T_e \sim 35$ eV in the MSh and $T_e \sim 60$ eV in the MpCL. Furthermore T_e (Thc) $\approx T_e$ (Tha) $\approx$60 eV in the MpCL, which confirms that magnetosheath electrons are heated in the MpCL. Figure 6 panel (e) displays an electron spectrogram from Thc. It shows how photoelectrons are removed, allowing a precise estimate of T_e in the various regions (see Fig. 6 panel d).

Howes et al. (2008) ran gyrokinetic simulations showing that the phase velocity of kinetic Alfvén waves (KAWs) gets much larger than V_a when $k_\perp \gg k_{//}$ and $k_\perp \rho_i \gg 1$. In this regime short (transverse) scale Alfvén waves (SSAWs) have a finite $E_{//}$ and can therefore interact efficiently with electrons via Landau damping, as will be discussed later. Sahraoui et al. (2008) analyzed magnetic field fluctuations measured in the solar wind by the Cluster spacecraft. They interpreted fluctuations/waves observed in the solar wind as Doppler-shifted SSAWs and gave evidence for a change in the slope of the spectrum at frequencies corresponding to the electron scale, which confirms that small transverse scale fluctuations ($k_\perp \rho_i \gg 1$) can be damped via a collisionless process involving electrons, namely Landau or cyclotron damping. Given the large amplitude (∼1 nT) of the waves observed in the MpCL, a turbulent cascade could occur and explain the generation of SSAWs. It is not clear, however,r that a turbulent cascade can develop in a spatially limited region such as the MpCL.

In Sect. 5, it will be shown that the sharp gradients observed at the MpCL can generate SSAWs through a linear instability, which does not preclude a non linear cascade from occurring if the wave amplitude gets large enough to overcome the effect of the inhomogeneity. SSAWs observed by Sahraoui et al. (2008) in the solar wind are strongly Doppler shifted. In the case of present observations the ion velocity V_d is comparable to the ion thermal velocity, but the Doppler shift is still large because $k_\perp \rho_i \gg 1$. Therefore the Doppler shift normalized to the proton gyrofrequency can be larger than unity: $k_\perp V_d / \Omega_H \sim (k_\perp \rho_i)(V_d / V_{thi}) \gg 1$. Thus the Doppler shift is likely to largely exceed the frequency in the plasma frame (see discussion section). Let us now investigate the effect of SSAWs on electrons.

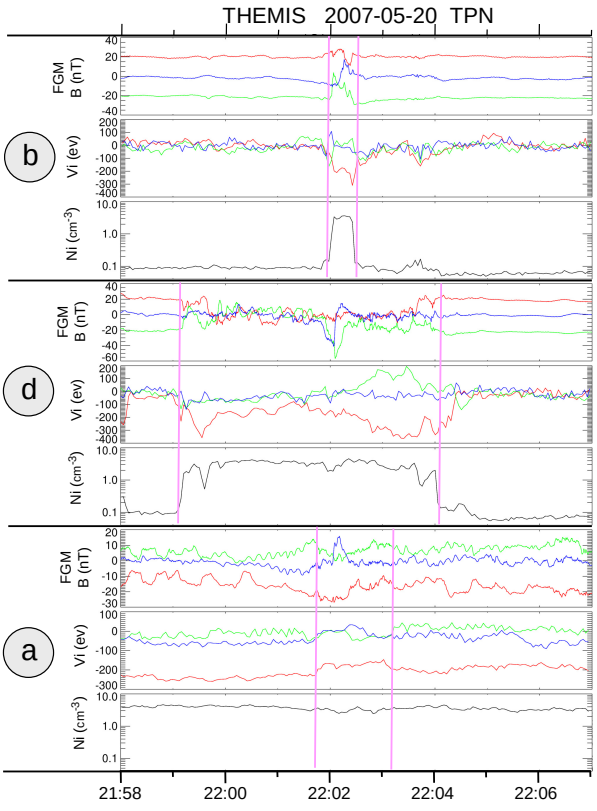

Fig. 5. Similar to Fig. 3, but TPN coordinates are used to display the magnetic field and the velocity. Notice that B_N and V_N are small on both sides of the event, as expected. The ion velocity is maximum on both sides of the FTE. Here red is for T, green for P and blue for N, the normal component.

4.3 Heating of particles by waves

In Fig. 3 the duration of the density ramp crossed while Thd penetratres the MpCL or gets out of it (at ∼21:59 and ∼22:04) is ∼12 s. The relative velocity between Thd and the magnetopause, measured along the normal (V_N), is ∼60 km s^{-1}, as estimated from Fig. 6. Hence the thickness of the density jump associated with the magnetopause is estimated to be L_N ∼720 km, which corresponds to about 7

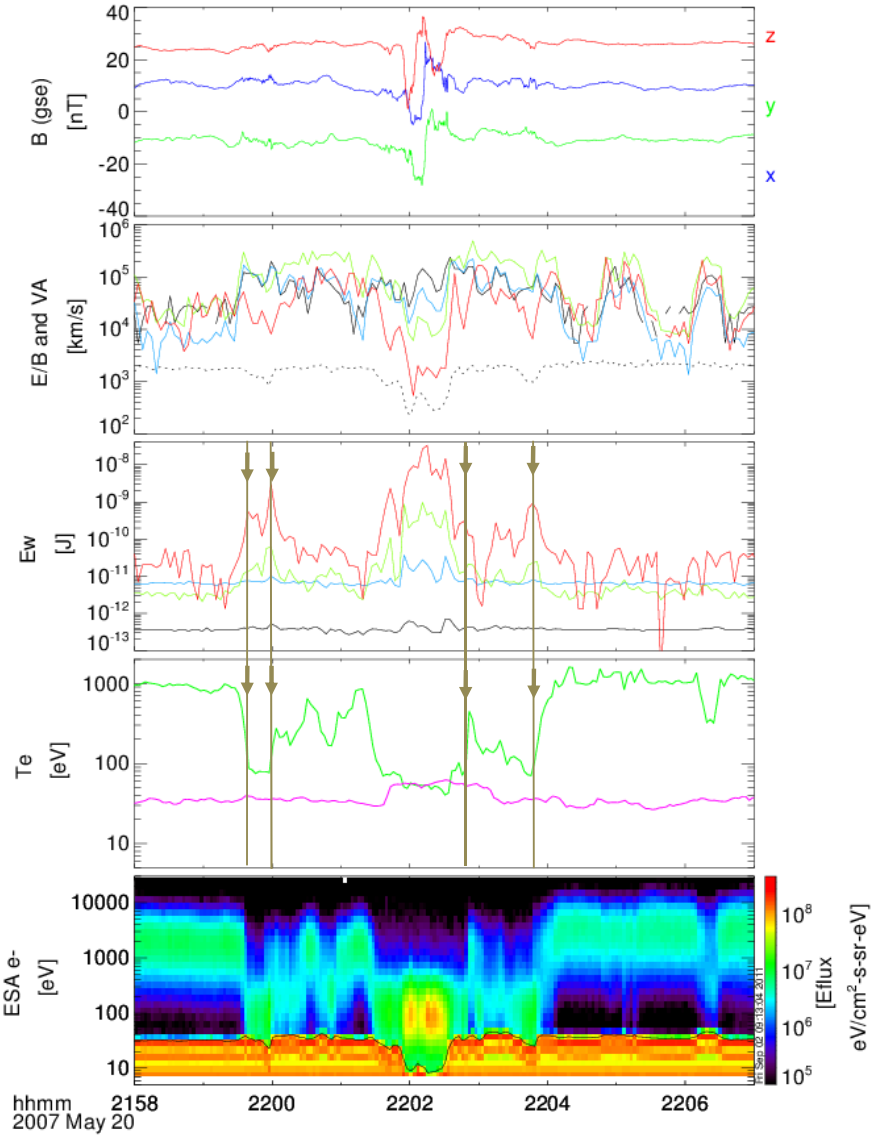

Fig. 6. This figure shows mainly data from Thc. From top to bottom: **(a)** the 3 components of the magnetic field, **(b)** $\delta E/\delta B$ for different frequencies (3 Hz in red, 12 in green, 48 in cyan and 192 Hz in black) and V_a (dotted line), **(c)** Ew the electromagnetic energy, **(d)** T_e for Thc (green) and Tha (magenta). The bottom panel shows a spectrogram from Thc; the spacecraft moves back and forth from the MSp to the MpCL. The thin vertical lines and superposed arrows point out the coincidences between sharp gradients in T_e and wave bursts.

ion Larmor radii of 400 eV ions. Given that we consider short wavelengths ($k_\perp \rho_i \gg 1$) we can, in first approximation, ignore the effect of the inhomogeneity and calculate the damping rate from using WHAMP software Rönnmark (1982). The role of the inhomogeneity will be further investigated in Sect. 5. Figure 7 shows the results of WHAMP for $T_i = 400$ eV, $T_e = 35$ eV, $N = 4\,\mathrm{cm}^{-3}$ (and hence $\beta_p \sim 6$, β being the ratio of the kinetic to the magnetic pressure), as estimated from data, for $1 < k_\perp \rho_i < 100$, $0.05 < k_{//} \rho_i < 0.15$, and $B_0 = 10$ nT. The real part of the dispersion relation obtained from WHAMP fits the expression given by Howes et al. (2008):

$$\omega = \frac{k_{//} V_a k_\perp \rho_i}{\sqrt{(\beta_p + 2)/(1 + T_e/T_i)}} \quad (1)$$

As expected, the imaginary part corresponds to damping, as illustrated in Fig. 7; the damping rate (red curve) becomes large as $k_\perp \rho_i$ increases. From the dispersion relation we find that $\omega/k_{//} V_i \sim 1$, (where V_i is the ion thermal velocity) is obtained for $k_\perp \rho_i \sim 7$, which corresponds to a very small ion Landau damping rate, according to Fig. 7. On the other hand, $\omega/k_{//} V_e \sim 1$ (V_e is the electron thermal velocity) is obtained for $k_\perp \rho_i \sim 90$, where the damping rate is very large. This rough comparison shows that ion Landau damping is weak

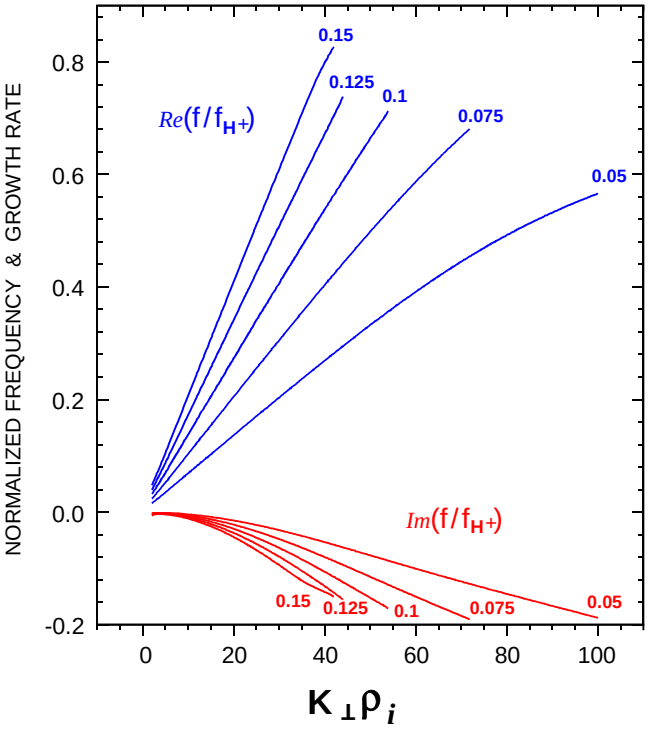

Fig. 7. Real (blue) and imaginary (red) part of the frequency normalized to the proton gyrofrequency, versus $k_\perp \rho_i$, for $k_{//}\rho_i$ between 0.05 and 0.015. For $k_\perp \rho_i \sim 1-10$ (ion scale) the damping rate is small, but it becomes large for $k_\perp \rho_i \sim 20$–100 (electron scale). Parameters are $N_i = 4\,\mathrm{cm}^{-3}$, $B_0 = 10\,\mathrm{nT}$, $T_e = 35\,\mathrm{eV}$, $T_i = 400\,\mathrm{eV}$; therefore $\beta = 6$.

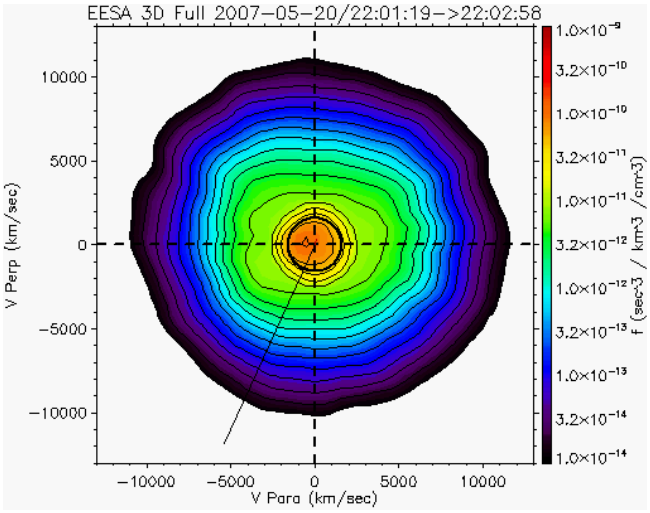

Fig. 8. Iso contours of the electron phase space density from Thd. At medium energies (green) evidence is given for $T_{e//} > T_{e\perp}$. Disregard the central region (red) which is influenced by photoelectrons.

while electron Landau damping is large, which explains why electrons are much more efficiently heated by SSAWs than ions.

The electron Landau damping tends to increase $T_{e//}$, the parallel electron temperature. Figure 8 gives evidence for an enhanced $T_{e//}$ as intense waves are observed, and it shows the electron distribution measured by Thd in the MpCL. As instrument is in the fast-survey mode, a full 3-D distribution needs ∼100 s. to be built. Yet the selected period does bracket the period in which intense waves are observed by Thd. Figure 8 shows an increase in the parallel temperature as compared to $T_{e\perp}$ and $T_{e//}$ in the MSh, which confirms that electrons are primarily heated by waves in the parallel (and anti-parallel) directions.

5 Wave generation

5.1 Drift wave instabilities

No relationship was found between temperature anisotropies and enhanced wave activity. On the other hand, the wave intensity increased as the spacecraft approached the magnetopause. The electromagnetic energy E_w is plotted on Fig. 6, panel (c). Figure 6, panels (c) and (d), gives evidence for the link between sharp T_e gradients (Fig. 6d) and wave energy bursts (Fig. 6c). As expected, E_w maximizes between 22:01:30 and 22:02:30 while Thc is inside the FTE. Secondary maxima (∼21:59:45 and ∼22:00:00, 22:02:50 and 22:03:45) are observed outside the FTE; they correspond to sharp gradients in T_e, as pointed out by arrows, in Fig. 6c and d. Weak gradients in T_e are not associated with peaks in E_w. Thus, the peaks in wave energy observed by Thc correspond to sharp gradients in T_e or to the FTE itself. It is therefore tempting to relate wave generation to drift effects associated with gradients. A wide variety of drift wave instabilities exists (Mikhailovskii, 1992). Driven by observations that give evidence of large magnetic components and large β, we consider electromagnetic instabilities in a high β plasma. Hasegawa (1971) showed that magnetosonic waves can be destabilized in high β plasmas in the presence of a density gradient and of a sufficient number of cold electrons. Because magnetosonic waves can have large $\omega/k_{//}$, they could be Landau damped by electrons and heat them. Yet a magnetosonic wave with $k_\perp \gg k_{//}$, should have δB along B, which does not fit present observations. In a high β plasma, instabilities driven by strong temperature gradients can develop; see a discussion by Aydemir et al. (1971) on drift instabilities in a high β plasma.

As pointed out above, THEMIS observations suggest that the observed waves are Alfvénic, propagate azimuthally, and have $k_\perp \gg k_{//}$ and $k_\perp \rho_i \gg 1$. This situation was considered by Mikhailovskii (1992, p. 100–102) who described the effect of temperature gradients on the dispersion relation of drift (kinetic) Alfvén waves with short perpendicular wavelengths. Let us analyze the dispersion relation of short scale

drift Alfvén waves (SSDAs) and determine the instability threshold. Mikhailovskii (1992) obtained the real and imaginary part of the dispersion relation of SSDAWs in a high β plasma for $k_\perp \rho_i \gg 1$ and a small $k_{//}\rho_i$. The key parameters are β; $T_\mathrm{i}/T_\mathrm{e}$; L_N the scale of the density gradient; the ratio between the gradients in T_i and T_e and the density gradients ($\eta_\mathrm{i} = \nabla T_\mathrm{i}/\nabla N$, and $\eta_\mathrm{e} = \nabla T_\mathrm{e}/\nabla N$), and $\alpha = \nabla B/\nabla N$, the ratio between the magnetic field and the density gradients. For simplicity we assume that electrons and ions are isotropic during at least the initial stage of the instability. The conservation of the total pressure is assumed, which provides a relation between these parameters.

For the sake of simplification Mikhailovskii took $\eta_\mathrm{i} = \eta_\mathrm{e}$. With this assumption he found that an instability develops for $\eta < -1$, that is for a temperature gradient steeper than the density gradient and in the opposite direction, as expected for the MSh/MSp interface. Given the large ratio between ion and electron Larmor radii, we expect steeper gradients in the electron temperature than in the ion temperature. Thus we have solved numerically the dispersion relation given by Mikhailovskii (1992) without assuming $\eta_\mathrm{i} = \eta_\mathrm{e}$. We restrict the analysis to parameters fitting present observations namely, temperature and density gradients in opposite directions (η_i and $\eta_\mathrm{e} < 0$), and $\alpha < 0$ (the latter comes from the conservation of the total pressure). The real part of the dispersion relation is given by (see Mikhailovskii, 1992, p. 32, formula 2.67):

$$D^{(0)} = \left(1 - \frac{\omega_\mathrm{ne}}{\omega}\right)\left(1 - \frac{\omega_\mathrm{ni}}{\omega}\right) + \frac{\beta}{2}\left(1 - \frac{\omega^*_\mathrm{pe}}{\omega}\right)\left(1 - \frac{\omega^*_\mathrm{pi}}{\omega}\right)$$

$$- \frac{c^2 k_\perp^2 k_z^2 \lambda_\mathrm{De}^2}{\omega^2}\left(1 + \frac{T_\mathrm{i}}{T_\mathrm{e}}\right) \qquad (2)$$

where

$$\omega_\mathrm{ne} = -\frac{c k_y T_\mathrm{e}}{e n_0 B_0}\frac{\partial n}{\partial x}$$

and

$$\omega_\mathrm{ni} = \frac{c k_y T_\mathrm{i}}{e n_0 B_0}\frac{\partial n}{\partial x}$$

λ_De is the Debye length.

For ω^*_pe and ω^*_pi null (no drift) we recover the dispersion relation of small transverse scale Alfvén wave (SSAWs). The first two terms describe the coupling with the drift. For a large β (here $\beta \sim 6$) the second term is generally larger than the first. Neglecting the last term we get two obvious solutions: $\omega = \omega^*_\mathrm{pi}$ and $\omega = \omega^*_\mathrm{pe}$ where

$$\omega^*_\mathrm{pi} = \frac{c k_y}{e n_0 B_0}\frac{\partial p_i}{\partial x}$$

and

$$\omega^*_\mathrm{pe} = -\frac{c k_y}{e n_0 B_0}\frac{\partial p_\mathrm{e}}{\partial x}$$

Equation (2) has only two roots; we select the one that corresponds to $\omega = \omega^*_\mathrm{pe}$ in the limit where the second drift term is dominant. Similarly, the imaginary part is classically determined by $\gamma = -i\,D^{(1)}/(\partial D^{(0)}/\partial\omega))$, where $D^{(1)}$ is given by Mikhailovskii (1992, p. 32, formula 2.68):

$$D^{(1)} = i\pi^{1/2}\frac{\omega}{|k_z|V_\mathrm{e}}\frac{T_\mathrm{i}}{T_\mathrm{e}}\left[\frac{\chi_1}{1+\frac{T_\mathrm{e}}{T_\mathrm{i}}}\left(2 + \frac{T_\mathrm{e}}{T_\mathrm{i}} - \frac{\omega_\mathrm{ne}}{\omega}\right)^2 + \right.$$

$$+ \beta_\mathrm{e}\left(2 + \frac{T_\mathrm{e}}{T_\mathrm{i}} - \frac{\omega_\mathrm{ne}}{\omega}\right)\left(1 - \frac{\omega^*_\mathrm{pi}}{\omega}\right)\chi_2 +$$

$$\left. + \frac{\beta_\mathrm{e}^2}{2}\left(1 + \frac{T_\mathrm{e}}{T_\mathrm{i}}\right)\left(1 - \frac{\omega^*_\mathrm{pi}}{\omega}\right)^2\chi_3\right] \qquad (3)$$

with

$$\chi_1 = 1 - \frac{\omega_\mathrm{ne}}{\omega}\left(1 - \frac{\eta_\mathrm{e}}{2}\right)$$

$$\chi_2 = 1 - \frac{\omega_\mathrm{ne}}{\omega}\left(1 + \frac{\eta_\mathrm{e}}{2}\right)$$

$$\chi_3 = 1 - \frac{\omega_\mathrm{ne}}{\omega}\left(1 + \frac{3}{2}\eta_\mathrm{e}\right)$$

and

$$\eta_\mathrm{e} = \frac{\partial \ln T_\mathrm{e}}{\partial \ln n_0} \qquad \beta_\mathrm{e} = \frac{8\pi n_0 T_\mathrm{e}}{B_0^2}$$

The real and imaginary parts of the frequency are computed numerically for parameters fitted with the data namely: $T_\mathrm{i} \sim 400$ eV, $T_\mathrm{e} \sim 35$ eV, $\beta = 6$, $B_0 = 10$ nT, $N = 4.10^6$ cm^{-3}, $L_\mathrm{N} = 10^6$ m, as functions of $k_\perp\rho_\mathrm{i}$ and for $0.05 < k_{//}\rho_\mathrm{i} < 0.125$. We limit ourselves to ∇T_e, ∇T_i, and ∇B inward (earthward), and ∇N outward (hence $\alpha < 0$). The corresponding results are presented in Fig. 9. For small values of $k_{//}$ ($k_{//}\rho_\mathrm{i} = 0.05$) the SSDAW is found to be unstable for $-1 < \eta_\mathrm{i} < 0$ and $\eta_\mathrm{e} < -2.5$. For a larger value of $k_{//}\rho_i$ there is still an instability but the threshold is more negative; for instance when $k_{//}\rho_\mathrm{i} = 0.1$ instability takes place for $(\eta_\mathrm{e})_\mathrm{min} < -3$, as indicated by the top RHS panel in Fig. 9. Frequencies are typically lower than or comparable to the proton gyrofrequency. Thus the electron mode is unstable for an electron temperature gradient steeper than the ion temperature gradient and oriented in a direction opposite to the density gradient. Given the large ratio between electron and ion Larmor radii, such a situation is expected to occur at the MP.

5.2 Discussion

The growth rate of drift waves is very sensitive to the scale of the gradients. For example if one divides the scales of these gradients by a factor of 2, the growth rate will be multiplied by a larger factor (> 2). The corresponding fast growth will lead to non-linear smoothing of the temperature profile. We therefore expect the drift wave to limit the sharpness of the profile to values on the order of 1000 km for

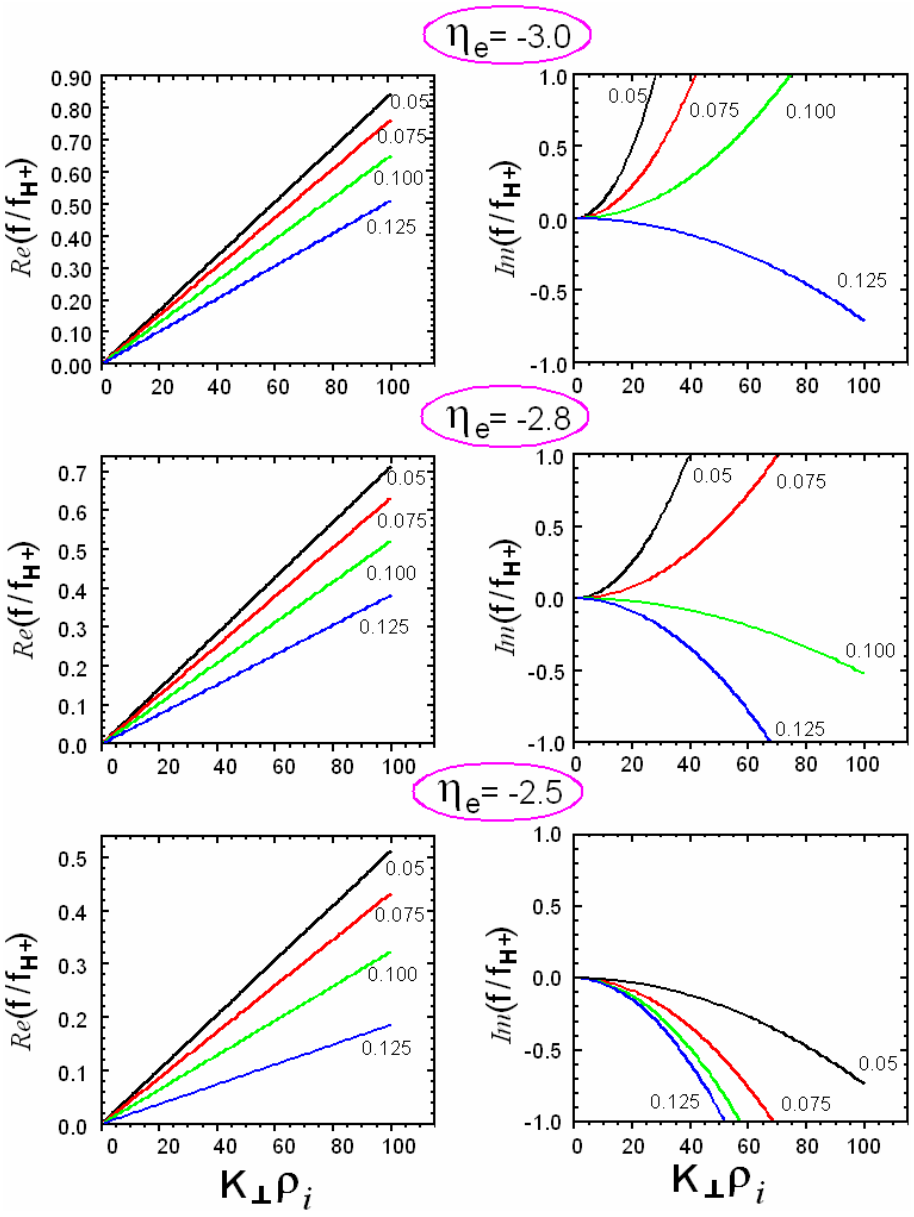

Fig. 9. Real and imaginary part of the normalized frequency versus $k_{\perp}\rho_{\rm i}$, for $0.05 < k_{//}\rho_{\rm i} < 0.125$. The inhomogeneity is now taken into account. Parameters are the same as for Fig. 7, except for inhomogeneity parameters: $\eta_{\rm e}$ (as indicated on the figure), $\alpha = -1.02, L_{\rm N} = 10^6$. For $\eta_{\rm e} > -2.5$, waves are damped, whatever $k_{//}\rho_{\rm i}$. For $\eta_{\rm e} < -2.5$ large growth rates are obtained, especially for the smaller values of $k_{//}\rho_{\rm i}$.

$L_{\rm N}$ and 2.5 times less for $L_{\rm Te}$ ($L_{\rm Te} \sim 400$ km). It turns out that this scale (400 km) is comparable to the ion Larmor radius of dominant ions (400 eV), with $\rho_{\rm i} \sim 200$ km. These estimates suggest that the MpCL thickness should have a lower bound ∼400–1000 km. Thus, spatial diffusion will tend to establish a MpCL thickness at equilibrium. This does not prevent Landau damping from occurring, however. As long as the linear growth rate of the drift instability ($\gamma_{\rm D}$) exceeds the modulus of the Landau damping ($|\gamma_{\rm L}|$), the wave will grow until non linear effects stabilize the drift instability. Assuming that quasi-linear theory applies, the spatial diffusion coefficient Dxx is proportional to E^2. For a steady state, the wave energy balance gives an equilibrium electric field E_c^2 proportional to $(\gamma_{\rm D} - |\gamma_{\rm L}|)/(k_{\perp}\rho_i)^2$. Note that $\gamma_{\rm D}$ grows faster with $k_{\perp}\rho_{\rm i}$ than $|\gamma_{\rm L}|$. Thus for a sufficiently large $k_{\perp}\rho_{\rm i}$, $\gamma_{\rm D}$ will always exceed $\gamma_{\rm L}$. The most unstable waves have $k_{\perp}\rho_i \gg 1$, which is consistent with the assumptions made to calculate the Landau damping (homogeneity) and the local approximation for drift-wave growth rate calculations ($\lambda_{\perp} \ll L_{\rm Te}$ and $L_{\rm Ne}$). We did not consider

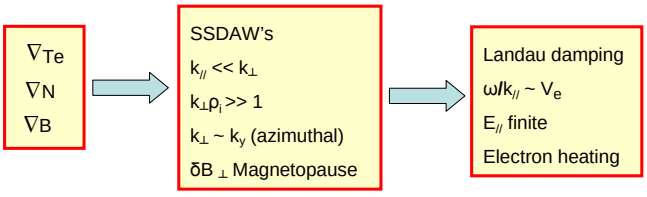

Fig. 10. Sketch summarizing our results. From the left to the right: appropriate gradients generate drift waves with small transverse scales. In turn these SSDAWs heat electrons.

the possibility that electrons (and ions) bounce along (reconnected) field lines. This is valid as long as a normal component has not yet developed; otherwise, damping would be related to bounce effect instead of the classical Landau damping. Similarly, curvature effects should be taken into account in the calculation of the drift wave growth rate.

It is interesting to evaluate the Doppler shift for the parameters used above. For $k_\perp \rho_\mathrm{i} = 50$ and $k_{//}\rho_\mathrm{i} = 0.1$, we find from the dispersion relation (1) that $\omega/\Omega_\mathrm{H} \approx 0.72$, which corresponds to a maximum Doppler shift:

$$\frac{\omega_\mathrm{Doppler}}{\Omega_{\mathrm{H}+}} \approx \frac{k_\perp V_{\mathrm{d\ max}}}{\Omega_\mathrm{H}} \approx \frac{k_\perp V_\mathrm{i}}{\Omega_\mathrm{H}} \approx k_\perp \rho_\mathrm{i} \approx 50 \qquad (4)$$

where we have assumed that $V_{\mathrm{d\ max}} \approx V_\mathrm{i}$, an assumption consistent with Fig. 5 panel (e). Thus the Doppler shift can be up to 70 times ω in the plasma frame for the parameters given above, which means that the wave instruments are measuring a k spectrum and are therefore probing scales. This is why the "spectrum" extension is so broad.

6 Conclusions

Intense electromagnetic waves observed in the magnetopause current layer and adjacent regions have been identified as short transverse scale Alfvén waves with parallel phase velocities much larger than V_a. We have shown that these waves can be driven unstable by a sharp earthward gradient in the electron temperature; we refer to them as short (transverse) scale drift Alfvén waves (SSDAWs). SSDAWs have $k\perp \gg k_{//}$ and therefore large parallel phase velocities and a small but finite $E_{//}$ were shown to be Landau damped by electrons. This damping is a likely explanation for the observed preferential heating of electrons in the presence of intense waves. SSDAWs have a dominant magnetic component normal to the MP and propagate azimuthally. They can break the frozen in condition and initiate turbulent magnetic reconnection. SSDAWs grow at the expense of gradients; they tend to reduce the sharpness of these gradients. Very large growth rates are obtained when the typical scale of those gradients becomes quite steep. For instance, when ∇T_e,∇T_i and ∇B are earthward and ∇N sunward (as expected for the MpCL), a large growth rate is found for an electron temperature gradient steeper than the density gradient. When $L_\mathrm{N} \sim 10^3$ km and $L_\mathrm{Te} \sim 4.10^2$ km, for example, SSDAs are strongly unstable, and can therefore produce fast spatial diffusion that levels out the gradients. This might explain why Berchem and Russell (1982) found an average magnetopause current layer thickness ~500 km. Note that most of the magnetopause crossings used by Berchem and Russell (1982) in their statistics correspond to large angles ($> 30°$) between magnetic fields inside and outside the magnetopause as it is the case in the present paper.

Figure 10, which summarizes our results, is a sketch describing wave generation and the effect of these waves on electron heating.

Acknowledgements. Support from THEMIS (NASA-NASS-02099) is acknowledged. French participation was funded by CNES. Present study was supported by CNRS and Ecole Polytechnique. The held of J. Hohl on editing the manuscript is acknowledged.

Guest Editor M. Taylor thanks two anonymous referees for their help in evaluating this paper.

The publication of this article is financed by CNRS-INSU.

References

Anderson, R. R., Harvey, C. C., Hoppe, M. M., Tsurutani, B. T., Eastman, T. E., and Etcheto, J.: Plasma waves near the magnetopause, J. Geophys. Rev., 87, 2087–2107, 1982.

Angelopoulos, V., Sibeck, D., Carlson, C. W., McFadden, J. P., Larson, D., Lin, R. P., Bonnell, J. W., Mozer, F. S., Ergun, R., Cully, C., Glassmeier, K. H., Auster, U., Roux, A., Le Contel, O., Frey, S., Phan, T., Mende, S., Frey, H., Donovan, E., Russell, C. T., Strangeway, R., Liu, J., Mann, I., Rae, J., Raeder, J., Li, X., Liu, W., Singer, H. J., Sergeev, V. A., Apatenkov, S., Parks, G., Fillingim, M., and Sigwarth, J.: The THEMIS Mission, Space Sci. Rev., 141, 5–34, doi:10.1007/s11214-008-9336-1, 2008.

Auster, H. U., Glassmeier, K. H., Magnes, W., Aydogar, O., Baumjohann, W., Constantinescu, D., Fischer, D., Fornacon, K. H., Georgescu, E., Harvey, P., Hillenmaier, O., Kroth, R., Ludlam, M., Narita, Y., Nakamura, R., Okrafka, K., Plaschke, F., Richter, I., Schwarzl, H., Stoll, B., Valavanoglou, A., and Wiedemann, M.: The THEMIS fluxgate magnetometer, Space Sci. Rev., 141, 509–534, doi:10.1007/s11214-008-9433-1, 2008.

Aydemir, A. Y., Berk, H. L., Mirnov, V., Pogutse, O. P., and Rosenbluth, M. N.: Linear and non linear description of drift instabilities in a high Beta plasma, Phys. Fluids, 30, 3083–3092, 1987.

Belmont, G. and Rezeau, L.: Magnetopause reconnection induced by magnetosheath Hall-MHD fluctuations, J. Geophys. Res., 106, 10751–10760, 2001.

Berchem, J. and Russell, C. T.: The thickness of the Magnetopause Current Layer: ISEE1 and 2 Observations, J. Geophys. Res., 87, 2108–2114, 1982.

Bonnell, J. W., Mozer, F. S., Delory, G. T., Hull, A. J., Ergun, R. E., Cully, C. M., and Angelopoulos, V.: The Electric Field Instrument (EFI) for THEMIS, Space Sci. Rev., 303–341, doi:10.1007/s11214-008-9469-2, 2008.

Chaston, C., Bonnell, J., McFadden, J. P., Carlson, C. W., Cully, C., Le Contel, O., Roux, A., Auster, H. U., Glassmeier, K. H., Angelopoulos, V., and Russell, C. T.: Turbulent heating and cross-field transport near the magnetopause from THEMIS, Geophys. Res. Lett., 35, L17S08, doi:10.1029/2008GL033601, 2008.

Cully, C. M., Ergun, R. E., Stevens, K., Nammari, A., and Westfall, J.: The THEMIS Digital Fields Board, Space Sci. Rev., 141, 303–341, doi:10.1007/s11214-008-9469-2, 2008.

Hall, D. S., Chaloner, C. P., Bryant, D. A., Lepine, D. R., and Tritakis, V. P.: Electrons in the boundary layer near the dayside magnetopause, J. Geophys. Res., 96, 7869–7891, 1991.

Hasegawa, A.: Drift-waves instabilities in a compressional high-beta plasma, Phys. Rev. Lett., 27, 11–14, 1971.

Howes, G. G., Dorland, W., Cowley, S. C., Hammett, G. W., Quataert, E., Schekochihin, A. A., and Tatsuno, T.: Kinetic simulations of magnetized turbulence in astrophysical plasmas, Phys. Rev. Lett., 100, 065004, doi:10.1103/PhysRevLett.100.065004, 2008.

Le Contel, O., Roux, A., Robert, P., Coillot, C., Bouabdellah, A., de la Porte, B., Alison, D., Ruocco, S., Angelopoulos, V., Bromund, K., Chaston, C. C., and Cully, C.: First results of THEMIS Search Coil Magnetometers (SCM): Space Sci. Rev., 141, 509–534, doi:10.1007/s11214-008-9371-y, 2008.

Mc Fadden, J. P., Carlson, C. W., Larson, D., and Angelopoulos, V.: THEMIS (ESA) first science results and performance issues, Space Sci. Rev., 141, 477–508, doi:10.1007/s11214-008-9433-1, 2008.

Mikhailovskii, A. B.: Electromagnetic instabilities in an inhomogeneous plasma, Plasma Physic series, edited by: Laing, E. W., Institute of Physics Publishing, Bristol, Philadelphia and New York, 1992.

Rezeau, L., Perraut, S., and Roux, A.: Electromagnetic fluctuations in the vicinity of the magnetopause, Geophys. Res. Lett., 13, 1093–1096, 1986.

Rezeau, L., Roux, A., and Russell, C. T.: Characterization of small-scale structures at the magnetopause from ISEE measurements, J. Geophys. Res., 98, 179–186, 1993.

Rönnmark, K.: WHAMP-Waves in homogeneous anisotropic multicomponent plasmas, Kiruna Geophysical Institute Report, 179, 1982.

Roux, A., Le Contel, O., Robert, P., Coillot, C., Bouabdellah, A., de la Porte, B., Alison, D., Ruocco, S., and Vassal, M. C.: The Search Coil Magnetometer (SCM) for THEMIS, Space Sci. Rev., 141, 265–275, doi:10.1007/s11214-008-9455-8, 2008.

Sahraoui, F., Goldstein, M. L., Robert, P., and Khotyaintsev, Yu. V.: Evidence of a cascade and dissipation of solar-wind turbulence at the electron gyroscale, Phys. Rev. Lett., 102, 231102, doi:10.1103/PhysRevLett.102.231102, 2008.

Sibeck, D. G., Kuznetsova, M., Angelopoulos, V., Glaßmeier, K.-H., and McFadden, J. P.: Crater FTEs: Simulation results and THEMIS observations, Geophys. Res. Lett., 35, L17S06, doi:10.1029/2008GL033568, 2008.

Stasiewicz, K., Khotyaintsev, Y., Berthomier, M., and Wahlund, J.-E.: Identification of widespread turbulence of dispersive Alfvén waves, Geophys. Res. Lett., 27, 173, 2000.

Tsyganenko, N. A.: On the re-distribution of the magnetic field and plasma in the near nightside magnetosphere during a substorm growth phase, Planet. Space Sci., 37, 183, 1989.